ACS APPLIED MATERIALS & INTERFACES

Research Article

www.acsami.org

Effective Visible-Excited Charge Separation in Silicate-Bridged ZnO/$BiVO_4$ Nanocomposite and Its Contribution to Enhanced Photocatalytic Activity

Xuedong Fu, Mingzheng Xie, Peng Luan, and Liqiang Jing*

Key Laboratory of Functional Inorganic Materials Chemistry, Ministry of Education, School of Chemistry and Materials Science, Heilongjiang University, Harbin 150080, P.R. China

Supporting Information

ABSTRACT: It is highly desired to enhance the visible-excited charge separation of nanosized $BiVO_4$ for utilization in photocatalysis. Here ZnO/$BiVO_4$ nanocomposites in different molar-ratios are fabricated by simple wet-chemical processes, after synthesis of nanosized $BiVO_4$ and ZnO by hydrothermal methods. It is shown by means of atmosphere-controlled steady-state surface photovoltage spectra and transient-state surface photovoltage responses that the photogenerated charges of resulting nanocomposite shows longer lifetime and higher separation than that of $BiVO_4$ alone. This leads to its superior photoactivities for water oxidation to produce O_2 and for colorless pollutant degradation under visible irradiation, with about three times enhancement. Interestingly, it is suggested that the prolonged lifetime and enhanced separation of photogenerated charges in the nanocomposite is attributed to the unusual spatial transfer of visible-excited high-energy electrons, by visible radiation from $BiVO_4$ to ZnO on the basis of the ultralow-temperature electron paramagnetic resonance measurements and the photocurrent action spectra. Moreover, it is clearly demonstrated that the photogenerated charge separation of resulting ZnO/$BiVO_4$ nanocomposite could be further enhanced after introducing the silicate bridges so as to improve the visible photocatalytic activity greatly, attributed to the built bridge favorable to charge transfer. This work would provide a feasible way to enhance the solar energy utilization of visible-response semiconductor photocatalysts.

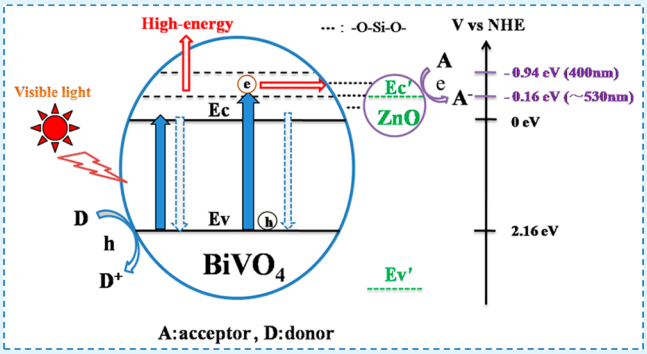

KEYWORDS: *ZnO/$BiVO_4$ nanocomposite, silicate bridge, photogenerated charge separation, water oxidation, visible photocatalysis*

1. INTRODUCTION

Nowadays, because of the increasingly environmental issues and the demand for renewable clean energy sources, semiconductor photocatalysis has drawn considerable attention.[1] Many semiconductors, such as $BiVO_4$,[2,3] Fe_2O_3,[4,5] Cu_2O,[6,7] and C_3N_4,[8,9] which have narrow band gap and can utilize the visible light in the solar spectrum, have been developed as photocatalysts. Among them, $BiVO_4$ (scheelite-monoclinic) has attracted attention as for its stability and nontoxicity, especially for its high activity for oxygen evolution in aqueous solutions in visible spectral range,[10] which is considered as the rate-determining step for water splitting. However, its photocatalytic activities for water oxidation and pollutant degradation are still not satisfactory. This is due to its conduction band bottom level being slightly positive to the proton reduction potential,[11] or the adsorbed O_2 reduction one,[12] so that the photogenerated electrons at conduction band bottom lacks sufficient reduction activities and thus easily recombines with the holes.[13,14] Up to now, great efforts have been made to enhance the photocatalytic activity of $BiVO_4$ with certain-degree successes, mainly by controlling the morphologies, such as nanotubes,[15] nanoplates,[16] nanoleaves,[17] core/shell nanowire,[18] nanoellipsoids,[19] special auxiliary structure,[20] and by doping with some elements, such as W,[21] Mo,[22] and P.[23] However, it is seldom involved with its low conduction band bottom issue in itself so that its visible activity is enhanced at a limited degree.

Recently, we have demonstrated that the visible activity of nanosized $BiVO_4$ for photocatalytic water splitting to evolve H_2 in the methanol solution is enhanced after coupling a small amount of nanocrystalline anatase TiO_2, in which the enhanced activity is attributed to the spatial transfers of visible-excited high-energy electrons (VE-HEEs) of $BiVO_4$ to TiO_2.[24] As for the so-called VE-HEE, its energy level is higher than that of the proton reduction potential. It is an unusual electron transfer process with great significance to improve the efficiency for utilizing VE-HEEs, which is completely different from the traditional way that the excited electrons of a semiconductor with high-level conduction band bottom would transfer to

Received: May 14, 2014
Accepted: October 12, 2014
Published: October 12, 2014

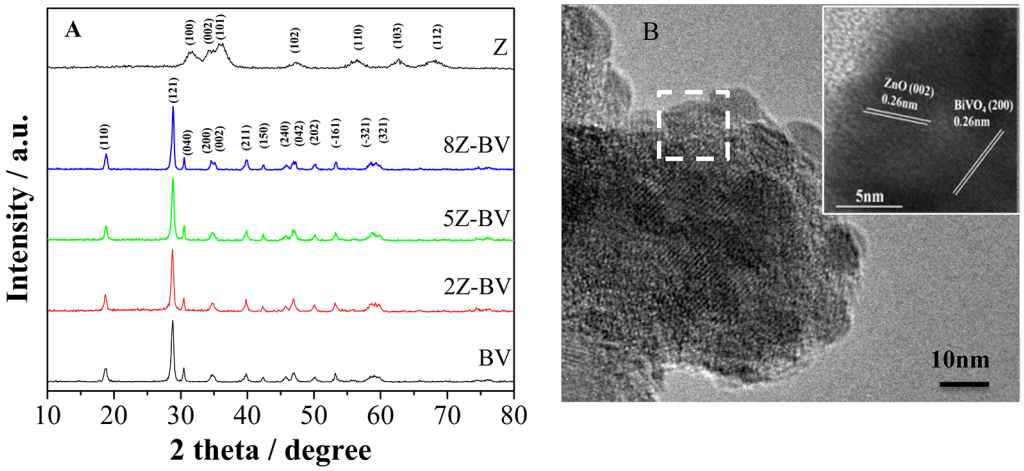

Figure 1. (A) XRD patterns, (B) TEM image (5Z-BV) with a HRTEM image as the inset. The samples were named as *X*Z-BV, in which Z is ZnO, BV is $BiVO_4$, and *X* is the molar content percentage of ZnO and $BiVO_4$.

another one with a low conduction band bottom level. Although the unusual electron transfer is energetically allowed, there is a great deal of VE-HEEs produced and phenomena similar to this were detected by Tang et al.,[25] recently, it is lacking of direct evidence. Noticeably, it is much meaningful to clarify the suggested transfer process.

In general, a wide-band gap oxide, like TiO_2 and ZnO, usually possesses a high-level conduction band bottom, at which photogenerated electrons with enough energy could effectively induce reduction reactions. Compared to TiO_2, ZnO has a similar band energy structure, and is also one of the most attractive materials for both fundamental research and industrial applications. However, it is much cheaper and relatively easy to prepare controllably.[26,27] In this case, it is much more expected that it is meaningful to couple $BiVO_4$ with ZnO in place of TiO_2. As it is known that, the formation of nanocomposite is usually influenced by the lattice matching degree and it is easy for the oxides with similar lattice parameters, to form the high-quality "connection" situation, which is much favorable for charge transfer. Because the lattice parameters of monoclinic $BiVO_4$[28] (a = 0.519 nm, b = 0.509 nm, c = 1.17 nm) and wurtzite ZnO[29] (a = 0.325 nm, c = 0.521 nm) are obviously different, it would require certain potential to improve the "connection" degree between these two parts. Particularly, silicate is mostly taken as one of the most effective modifiers as adhesives.[30−32] So, it will be feasible that the silicate would be taken as effective electron bridges for heterojunctional nanocomposite to promote charge transfer.

On the basis of above considerations, we are fabricating nanocrystalline ZnO-coupled $BiVO_4$, aiming to clarify the above suggested electron transfer processes. Herein, it is clearly demonstrated that the resulting ZnO/$BiVO_4$ nanocomposite will exhibits three-times higher photoactivities for water oxidation to produce O_2 and for colorless pollutant degradation in visible spectral region, compared to $BiVO_4$ alone, especially for the constructed silicate-bridged nanocomposite. Interestingly, it is confirmed for the first time that the obviously enhanced visible activities are attributed to the unusual spatial transfers of VE-HEEs of $BiVO_4$ to ZnO. This work will help us to understand deeply the unusually photophysical processes and will also provide a feasible route to enhance the solar energy utilization of semiconductor photocatalysis.

2. EXPERIMENTAL SECTION

All substances used in this study were analytical grade and without further purification and deionized water was used in all experiments.

2.1. Preparation of Materials. Nanosized $BiVO_4$ was prepared through an EDTA-modified hydrothermal process in our previous publication,[33] and ZnO was carried out through a colloidal method.[34] The nanocomposites of ZnO-coupled $BiVO_4$ and silicate-bridged ZnO/$BiVO_4$ were prepared by the wet chemical method. Related detail procedures were described in the Supporting Information.

2.2. Preparation of Film Electrodes. To carry out PEC measurements, we prepared corresponding pastes by the similar process,[35] which was described in detail in the Supporting Information.

2.3. Characterization of Materials. The samples were characterized by X-ray diffraction (XRD) with a Rigaku D/MAX-rA diffractometer (Japan), using Cu−Kα radiation (λ = 0.15418 nm), and an accelerating voltage of 30 kV and emission current of 20 mA were employed. The UV−vis diffuse reflectance spectra (DRS) of the samples were recorded with a Model Shimadzu UV-2550 spectrophotometer. Electron micrographs were taken on a JEOL JEM-2100 transmission electron microscope (TEM) operated at 200 kV. Raman spectra were recorded by a Jobin Yvon HR800 micro-Raman spectrometer with 457.9 nm laser, and the laser intensity at the sample was kept below the threshold for any laser-induced changes in the Raman spectra and electrical transport characteristics. The nanocomposites powders were placed on a clean SiO_2/Si substrate for the Raman measurement.

The steady-state surface photovoltage spectroscopy instrument was a home-built apparatus equipped with a lock-in amplifier (SR830) synchronized with a light chopper (SR540).[36] Transient-state surface photovoltage measurement was performed with a self-assembled device in air atmosphere at room temperature.[36] The related apparatuses and measurement methods for the steady-state surface photovoltage spectroscopy and transient-state surface photovoltage responses, for produced hydroxyl radical amount, and for electron paramagnetic resonance were described in the Supporting Information.

2.4. Photoelectrochemical (PEC) Experiments. PEC experiments were performed in a glass cell using 500 W xenon lamp with an intensity of 64 mW/cm^2 after ultilizing a filter to remove the light with wavelength shorter than 420 nm as light resource and 0.5 M $NaClO_4$ (pH 7.0) solution as electrolyte. The as-prepared films were used as working electrodes (0.25 cm^2), illuminated from the FTO glass side (illuminated from the sample side in the measurement for the samples with different layers (see Figure S6 in the Supporting Information). Platinum plate (99.9%) was used as the counter electrode, and a saturated KCl Ag/AgCl electrode was used as the reference electrode. High-purity N_2 gas was used to bubble through the electrolyte before and during the experiments. Applied potentials were controlled by a

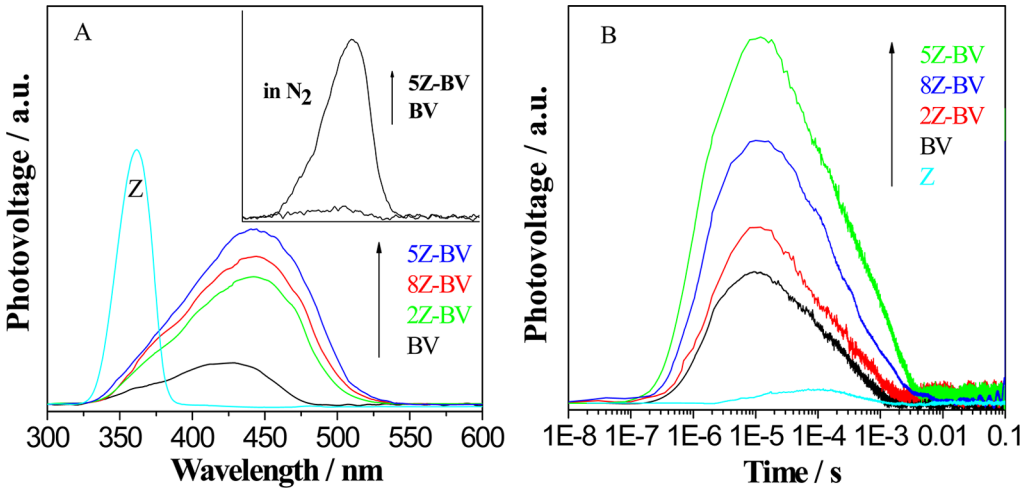

Figure 2. (A) Steady-state surface photovoltage spectra and (B) transient-state surface photovoltage responses of different ZnO/$BiVO_4$ nanocomposites in air. The inset shows the steady-state surface photovoltage spectroscopy responses in N_2.

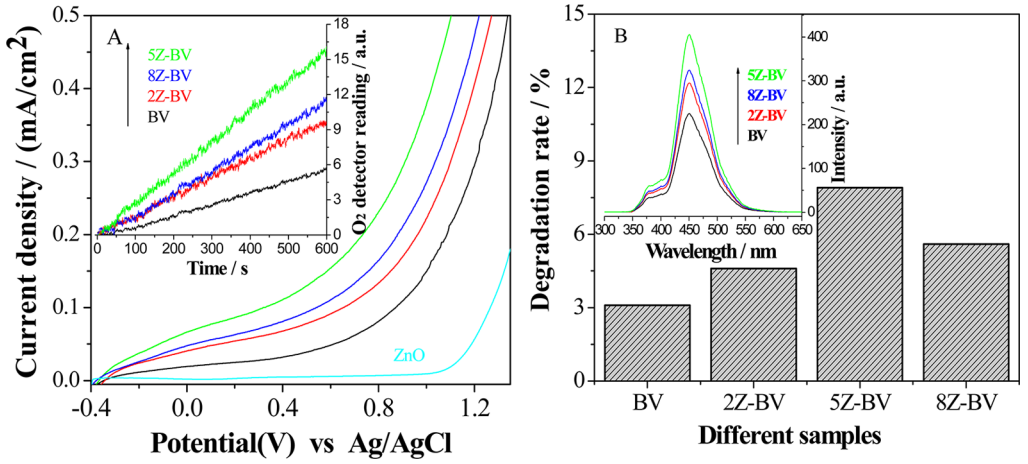

Figure 3. (A) *I*–*V* curves with the temporal produced O_2 amount as the inset. (B) Photocatalytic activity for degrading liquid-phase phenol; inset shows the fluorescence spectra. PEC performance is measured in the 0.5 M $NaClO_4$ electrolyte (pH 7.0). A three-electrode cell is used with the testing film as the working electrode, an Ag/AgCl (saturated KCl solution) electrode as the reference, and Pt plate as the counter electrode. All measurements are under visible irradiation.

commercial computer-controlled potentiostat (LK2006A made in China). The PEC procedures to measure the O_2 amount and Nyquist plots were described in the Supporting Information.

2.5. Photocatalytic Activity Evaluation. This is described in the Supporting Information.

3. RESULTS AND DISCUSSION

3.1. Phase Composition and Structural Characterization. According to the XRD patterns in Figure 1A, it is confirmed that the resulting ZnO is nanocrystalline, with the wurtzite structure.[37] One can also notice that the introduction of a small amount of ZnO does not change the crystal phase, which is also supported by the Raman spectra (see Figure S1A in the Supporting Information), and crystallinity of monoclinic $BiVO_4$. Similarly, its optical absorption across band gap energy on the basis of UV–vis diffuse reflectance spectra nearly keeps unchanged (see Figure S1B in the Supporting Information). On the basis of the TEM image of resulting nanocomposite (Figure 1B), it is seen that the spherical-like ZnO nanoparticles with about 5 nm (see Figure S2A in the Supporting Information) are dispersed uniformly on the surfaces of nanosized $BiVO_4$ with about 60 nm (see Figure S2B in the Supporting Information) in diameter, and the intimate heterojunction is formed between ZnO and $BiVO_4$ by means of the facet distances of 0.26 and 0.26 nm in the inset, respectively, corresponding to ZnO (002) and $BiVO_4$ (200) facets. It is widely acceptable that the close contacts between different constituents in the fabricated nanocomposite are favorable for charge transfer and separation.

3.2. Photogenerated Charge Separation. The photogenerated charge carrier properties of $BiVO_4$ and ZnO/$BiVO_4$ nanocomposites were investigated by atmosphere-controlled steady-state surface photovoltage spectroscopy response. As shown in Figure S3A in the Supporting Information, there is no signal in the absence of O_2, and with higher O_2 concentration, the response increases. Hence, it is deduced that the response of $BiVO_4$ greatly depends on the O_2 concentration, in accordance with our previous work.[24] This is attributed to the action of adsorbed O_2 for capturing photogenerated electrons. As for ZnO/$BiVO_4$, although its steady-state surface photovoltage spectroscopy response is proportional to O_2 concentration, it is still detectable in N_2 (see Figure S3B in the Supporting Information and Figure 2A inset). This is possibly related to the charge transfer from $BiVO_4$ to ZnO. It is clearly seen from Figure 2A, as the amount of coupled ZnO

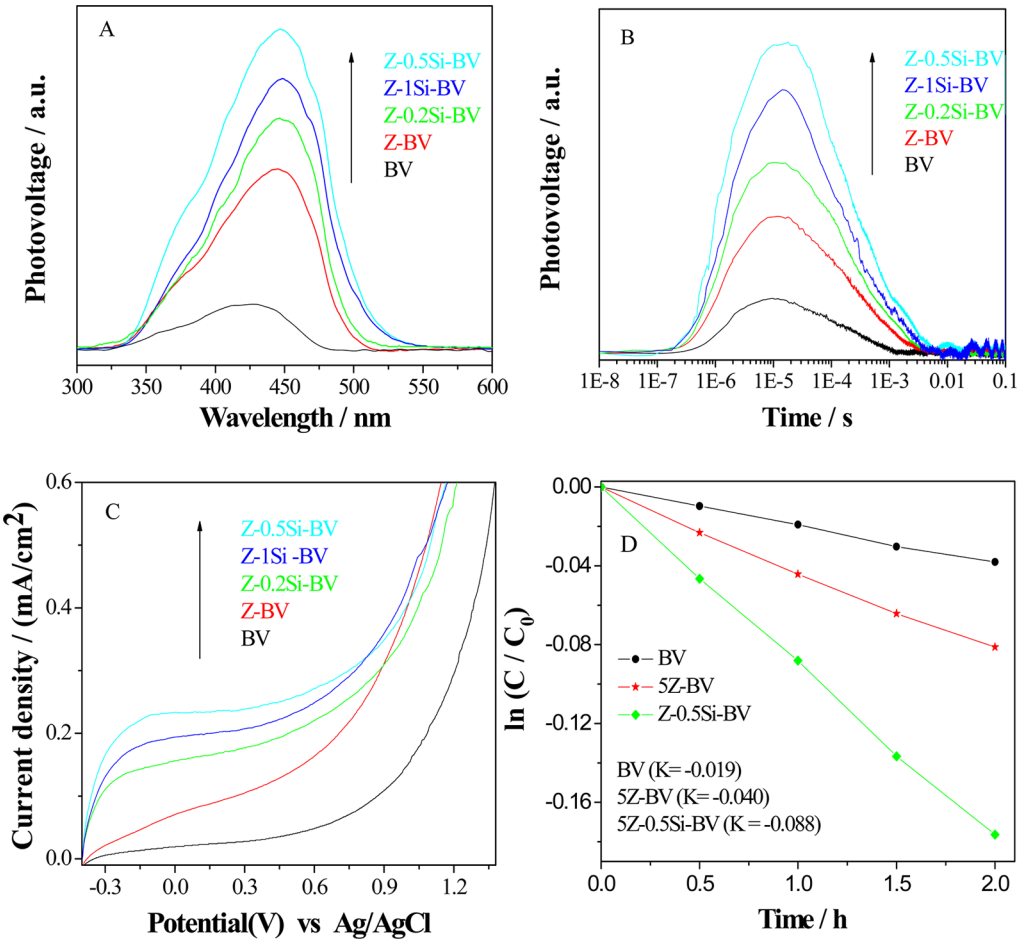

Figure 4. (A) Steady-state surface photovoltage spectroscopy and (B) transient-state surface photovoltage responses in air, (C) *I*−*V* curves under visible irradiation, and (D) photocatalytic activity for degrading phenol of different silicate-bridged ZnO/$BiVO_4$ nanocomposites.

increases, the steady-state surface photovoltage spectroscopy response becomes gradually stronger. For the 5Z-BV sample, it exhibits the strongest response. If the ZnO amount is continuously increased, the response begins to decrease. This is because excess ZnO is unfavorable for optical adsorption.

The above steady-state surface photovoltage spectroscopy results are further supported by the recorded transient-state surface photovoltage responses (Figure 2B). In particular, it is noticed that the transient-state surface photovoltage response of $BiVO_4$ are enhanced markedly after coupling with a proper amount of ZnO, and the strongest response is observed for the 5Z-BV sample. It is worthy of note that the lifetime of the photogenerated charge was also prolonged by several seconds. This is in good agreement with the steady-state surface photovoltage spectroscopy response. On the basis of the obviously enhanced transient-state surface photovoltage responses and the prolonged charge lifetime, it is confirmed that the separation of photogenerated charge carriers of nanosized $BiVO_4$ could be considerably improved by coupling with a proper amount of nanocrystalline ZnO. Similar to TiO_2,[24] ZnO displays a weak transient-state surface photovoltage response under visible laser excitement, which results from its surface states on the basis of the UV−vis diffuse reflectance spectra (see Figure S1B in the Supporting Information).

3.3. Visible Activities for PEC Water Oxidation and Pollutant Degradation. The separation of photogenerated charge carriers of $BiVO_4$ would be greatly enhanced by coupling with ZnO based on the steady-state surface photovoltage spectroscopy responses in N_2 and air. It is anticipated that the resulting ZnO/$BiVO_4$ nanocomposites would exhibit high visible photoactivity. To prove the anticipation, we first carry out the photoelectrochemical experiments. As shown in Figure S4A, B in the Supporting Information, the introduction of a small amount of ZnO does not change the crystal phase, crystallinity and optical absorption of nanosized $BiVO_4$ film, whereas it exhibits slight effects on the dark current (see Figure S5A in the Supporting Informatio). One can see from Figure 3A that the photocurrent density of $BiVO_4$ film is rather small under visible irradiation, and it could be enhanced after coupling with a proper amount of ZnO. Among the fabricated ZnO/$BiVO_4$ nanocomposites, the 5Z-BV one shows the largest photocurrent density at the applied voltage of 0.4 V (vs RHE), which is about three times larger than the $BiVO_4$ alone. This is in good agreement with the decreased arc in the Nyquist plot under visible irradiation (see Figure S5B in the Supporting Information). Generally speaking, large photocurrent density corresponds to high photocatalytic activity for water oxidation to evlove O_2. As expected, the amount of evolved O_2 on the basis of inset in Figure 3 A is fully consistent with the corresponding photocurrent density, and 5Z-BV is the largest amount of produced O_2 under visible illumination for the ZnO/$BiVO_4$ nanocomposite.

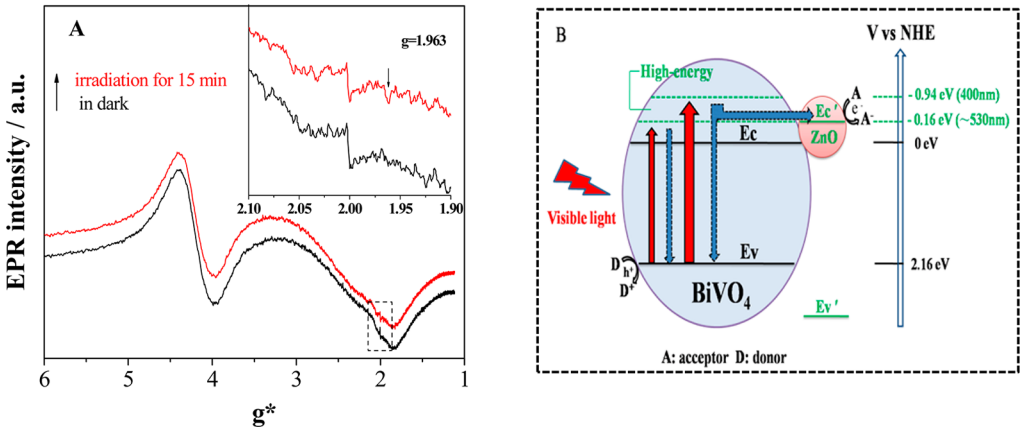

Figure 5. (A) Electron paramagnetic resonance responses of 5Z-BV at 1.8K. The sample was irradiated by the laser beam with wavelength of 532 nm and power of 5W. (B) Process schematic of transfer and separation of visible-excited high-energy electrons for the fabricated ZnO/$BiVO_4$ nanocomposite. Ev and Ec represent the valence band and the conduction band of $BiVO_4$, Ev′ and Ec′ represent the valence band and the conduction band of ZnO respectively.[41,42] High-energy electrons are located at the visible light range from 400 to 530 nm.

Moreover, the enhanced visible activity is also supported by degradation of liquid-phase phenol (Figure 3B) and gas-phase acetaldehyde (see Figure S6 in the Supporting Information). It is confirmed that, among the resulting nanocomposites, the 5Z-BV sample exhibits the highest visible activity for degrading phenol and acetaldehyde. In general, hydroxyl radical (·OH) is taken as important active species in the photocatalytic degradation of liquid-phase pollutants, and the larger is the produced ·OH amount, the higher is the photocatalytic activity.[38] The coumarin fluorescent method, a highly sensitive technique, is frequently used to detect ·OH. In this the introduced coumarin easily reacts with ·OH to produce luminescent 7-hydroxycoumarin at about 460 nm.[38] It is confirmed from the inset in Figure 3B that the intensity of fluorescent signal related to the amount of produced ·OH is highly responsible for the visible activity for degrading phenol. Therefore, it is clearly demonstrated that the visible photoactivities of nanosized $BiVO_4$ could be enhanced greatly after coupling with a proper amount of nanocrystalline ZnO.

3.4. Effects of Silicate Bridges. As discussed above in introduction, it is possible and meaningful to improve the connections between ZnO and $BiVO_4$, which would be beneficial for effective charge transfers in the fabricated nanocomposite. On the basis of the XRD patterns (see Figure S7A in the Supporting Information), diffuse reflectance spectra (see Figure S7B in the Supporting Information) and TEM image (see Figure S8 in the Supporting Information), it is found that the silicate introduction does not change the crystal phase, crystallinity, and the morphology of ZnO/$BiVO_4$ nanocomposites. According to the FT-IR spectra (see Figure S9A in the Supporting Information), it is confirmed that a new peak is observed at about 1050 cm^{-1} for the silicate-bridged nanocomposite, resulting from the Si−O−Si mode.[40] It is noted from panels A and B in Figure 4 that after a proper amount of silicate is introduced as electron bridges, the steady-state surface photovoltage spectroscopy and transient-state surface photovoltage responses of ZnO/$BiVO_4$ nanocomposite are greatly increased also including in N_2 (see Figure S9B in the Supporting Information), indicating that the photogenerated charge separation is considerably enhanced. As shown in Figure S10A,B in the Supporting Information the silicate introduction does not change the crystal phase, crystallinity and optical absorption of ZnO/$BiVO_4$ film, whereas it exhibits slight effects on the dark current (see Figure S11A in the Supporting Information). Obviously, it could enhance the visible photocurrent density two times, especially for the Z-0.5Si−BV as compared to the ZnO/$BiVO_4$ (Figure 4C). This is in good agreement with the amounts of evloved O_2 in the PEC water oxidation (see Figure S11B in the Supporting Information). In addition, the IPCE analysis (see Figure S12 in the Supporting Information) shows that the Z-0.5Si−BV nanocomposite achieves 10% at 400 nm, about three times than bare $BiVO_4$. As expected, it is also supported by the visible photocatalytic activities for degrading liquid-phase phenol (Figure 4D) and gas-phase acetaldehyde (see Figure S13 in the Supporting Information).

3.5. Discussion of Mechanisms. On the basis of analyses, it is confirmed that the introduction of nanocrystalline ZnO would prolong the lifetime and promote the separation of photogenerated charges of nanosized $BiVO_4$, leading to highly improving visible activities for PEC water oxidation to produce O_2 and degradation of colorless pollutant. What results in the enhancement of charge separation? It is assumed that the charge separation enhancement is attributed to the transfers of VE-HEEs of $BiVO_4$ to ZnO in the fabricated nanocomposite. To clarify the assumption, we have carried out the measurements of electron-spin resonance at the ultralow-temperature (1.8 k) of the representative 5Z-BV nanocomposite. As shown in Figure 5A, that both of the two samples in dark show the same peaks, resulting from $BiVO_4$, while the characteristic peak of Zn^+ in ZnO at g = 1.963 is not detected from Figure 5 A inset.[39] After it is irradiated by the visible laser of 532 nm for 15 min, a new electron paramagnetic resonance peak at g = 1.963 appears. Thus, it is evidently demonstrated by the so produced Zn^+, that the spatial transfers of VE-HEEs from $BiVO_4$ to ZnO take place in the nanocomposite because ZnO could not be excited. In fact, it is difficult to catch the significant electron paramagnetic resonance signal of Zn^+ in 5Z-BV because no change is observed for electron paramagnetic resonance signals before and after visible laser excitation at room temperature, even at liquid-N_2 temperature. To further support the VE-HEE transfers in space, we have designed a PEC experiments. The $I-V$ curves of the fabricated $BiVO_4$/ZnO/FTO film, irradiated from the $BiVO_4$ side, are performed (see Figure S14 in the Supporting Information). It is found that the presence of thin ZnO layer between FTO and $BiVO_4$ enhances the photo-

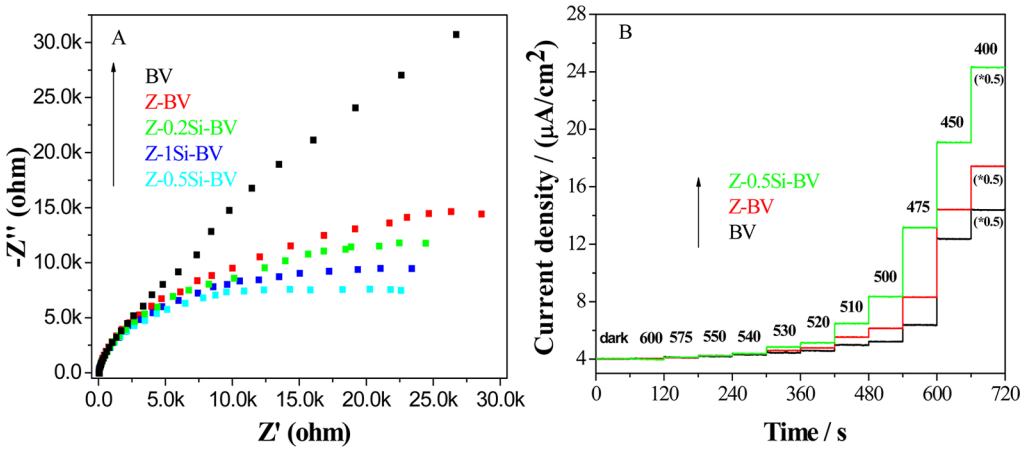

Figure 6. (A) Electrochemical impedance spectroscopy Nyquist plots under visible irradiation, and (B) normalized photocurrent action spectra vs visible excitation wavelength at 0.4 V bias vs Ag/AgCl. The photocurrents under excitation with wavelength of 400 nm were shown as the half of the original data.

current density of $BiVO_4$ under visible irradiation. This is attributed to the charge transfer from $BiVO_4$ to ZnO so as to promote the visible-excited charge separation of $BiVO_4$.

On the basis of above results, a mechanism schematic is emerged as Figure 5B. Thus, it is clear that, when $BiVO_4$ is excited under visible illumination, lots of VE-HEEs (from 530 to 400 nm) would be generated. Actually, these high-energy electrons are active for inducing reduction reactions. If there is $BiVO_4$ alone, the VE-HEEs would quickly relax to its conduction band bottom level so as to greatly decrease the reaction activity. On the other side, if ZnO is coupled, the VE-HEEs would thermodynamically transfer to ZnO so as to still maintain the relatively high energy level. This would be much favorable to prolong the lifetime, to promote the separation, and to induce oxidation/reduction reactions of visible-excited charges. To further prove the suggested mechanism, we also fabricate the 5Z-BV nanocomposite by mixing mechanically. As expected, the mechanically fabricated nanocomposite displays slightly low steady-state surface photovoltage spectroscopy response (see Figure S15A in the Supporting Information) and small photocurrent density (see Figure S15B in the Supporting Information), compared to $BiVO_4$ alone. This is attributed to the weak contacts between ZnO and $BiVO_4$. In addition, it is demonstrated that the small nanoparticle size for ZnO is much more beneficial for charge transfers of fabricated ZnO/$BiVO_4$ nanocomposite (see Figure S16 in the Supporting Information). This is also related to the constituent-contacted situation since the ZnO nanosize does not influence the optical absorption. Therefore, it is understandable that the fabricated ZnO/$BiVO_4$ nanocomposite would exhibit much higher photocatalytic activities than $BiVO_4$ alone, and the constituent-contacted situation is crucial for effective charge transfer and separation in the fabricated nanocomposite.

As mentioned above, the introducing of silicate is beneficial to improve the photocatalytic performance of ZnO/$BiVO_4$. It is mainly attributed to the introduced silicate, which is favorable for charge transfer and clarified by the decreased Nyquist arc radius under visible irradiation (Figure 6A). It is noticed from the photocurrent action spectra as a function of visible wavelength at the applied voltage of 0.4 V (Figure 6B) that the normalized photocurrent gradually increases with decreasing the irradiation wavelength, closely related to the increased energy levels of excited electrons. In particular, the 5Z-BV and Z-0.5Si-BV nanocomposites show an obvious enhancement of photocurrent density below 530 nm compared with the $BiVO_4$ alone. This is because the photogenerated electrons below 530 nm are allowed energetically to transfer to ZnO in space. To further illustrate the effects of introduced silicate, we showed the blank experiments of silicate/$BiVO_4$ composite in Figure S17A, B in the Supporting Information. On the basis of the surface photovoltage spectroscopy responses and the observed photocurrent densities, it is clearly confirmed that it is unfavorable for $BiVO_4$ to introduce the silicate. Hence, it is believable that the introduced silicate would act as a electronic bridge for charge transfer from $BiVO_4$ to ZnO under visible irradiation.

4. CONCLUSIONS

On the basis of the systematical investigation, the following conclusions could be drawn: (i) Different ZnO/$BiVO_4$ nanocomposites are successfully fabricated by a simple wet-chemical process. (ii) The lifetime and the separation of photogenerated charge carriers of nanosized $BiVO_4$ could be greatly increased after coupling with a proper amount of nanocrystalline ZnO, attributed to the unusual spatial transfers of visible-excited high-energy electrons from $BiVO_4$ to ZnO. (iii) Interestingly, the resulting ZnO/$BiVO_4$ nanocomposite could exhibit much higher visible activities for PEC water oxidation to produce O_2 and for colorless pollutant degradation than $BiVO_4$ alone. (iv) The silicate bridge would be favorable to improve the effective connections between different constituents, so as to promote charge transfer and separation in the resulting ZnO/$BiVO_4$ nanocomposite, leading to the improved photoactivities. Obviously, this work would provide a feasible way to enhance the solar energy utilization of visible-response semiconductor photocatalysts.

■ ASSOCIATED CONTENT

Supporting Information

Experimental; Figure S1, Raman spectra and UV−vis diffuse reflectance spectra; Figure S2, TEM images; Figure S3, steady-state surface photovoltage spectroscopy responses; Figure S4, XRD patterns and UV−vis diffuse reflectance spectra; Figure S5, *I*−*V* curves and Electrochemical impedance spectra; Figure S6, photocatalytic activity; Figure S7, XRD patterns and UV−vis diffuse reflectance spectra; Figure S8, TEM image; Figure

S9, FT-IR spectra and steady-state surface photovoltage spectroscopy responses; Figure S10, XRD patterns and UV−vis diffuse reflectance spectra; Figure S11, *I*−*V* curves and the temporal produced O_2 amount; Figure S12, IPCE curves; Figure S13, photocatalytic activity; Figure S14, *I*−*V* curve; Figure S15, steady-state surface photovoltage spectroscopy responses and *I*−*V* curves; Figure S16, XRD patterns, UV−vis diffuse reflectance spectra steady-state surface photovoltage spectroscopy responses, and *I*−*V* curves; Figure S17, steady-state surface photovoltage spectroscopy responses and *I*−*V* curves. This material is available free of charge via the Internet at http://pubs.acs.org.

AUTHOR INFORMATION

Corresponding Author

*E-mail: Jinglq@hlju.edu.cn.

Notes

The authors declare no competing financial interest.

ACKNOWLEDGMENTS

We are grateful for financial support from NSFC (21071048), the National Key Basic Research Program of China (2014CB660814), the Program for Innovative Research Team in Chinese Universities (IRT1237), the Project of Chinese Ministry of Education (213011A), the Specialized Research Fund for the Doctoral Program of Higher Education (20122301110002), the Chang Jiang Scholar Candidates Programme for Heilongjiang Universities (2012CJHB003), and the Science Foundation for Excellent Youth of Harbin City of China (2014RFYXJ002).

REFERENCES

(1) Cao, S. W.; Yin, Z.; Barber, J.; Boey, F. Y. C.; Loo, S. C. J.; Xue, C. Preparation of Au-$BiVO_4$ Heterogeneous Nanostructures as Highly Efficient Visible-Light Photocatalysts. *ACS Appl. Mater. Interfaces* **2012**, *4*, 418−423.

(2) Li, R. G.; Han, H. X.; Zhang, F. X.; Wang, D. G.; Li, C. Highly efficient Photocatalysts Constructed by Rational Assembly of Dual-cocatalysts Separately on Different Facets of $BiVO_4$. *Energy Environ. Sci.* **2014**, *7*, 1369−1376.

(3) Seabold, J. A.; Choi, K. S. Efficient and Stable Photo-Oxidation of Water by a Bismuth Vanadate Photoanode Coupled with an Iron Oxyhydroxide Oxygen Evolution Catalyst. *J. Am. Chem. Soc.* **2012**, *134*, 2186−2192.

(4) Hou, Y.; Zuo, F.; Dagg, A.; Feng, P. Y. Visible Light-Driven α-Fe_2O_3 Nanorod/Graphene/$BiV_{1-x}Mo_xO_4$ Core/Shell Heterojunction Array for Efficient Photoelectrochemical Water Splitting. *Nano Lett.* **2012**, *12*, 6464−6473.

(5) Sivula, K.; Zboril, R.; Formal, F. L.; Robert, R.; Weidenkaff, A.; Tucek, J.; Frydrych, J.; Grätzel, M. Photoelectrochemical Water Splitting with Mesoporous Hematite Prepared by a Solution-Based Colloidal Approach. *J. Am. Chem. Soc.* **2010**, *132*, 7436−7444.

(6) Li, J. T.; Cushing, S. K.; Bright, J.; Meng, F. K.; Senty, T. R.; Zheng, P.; Bristow, A. D.; Wu, N. Q. Ag@Cu_2O Core-Shell Nanoparticles as Visible-Light Plasmonic Photocatalysts. *ACS Catal.* **2013**, *3*, 47−51.

(7) Wang, D. G.; Li, R. G.; Zhu, J.; Shi, J. Y.; Han, J. F.; Zong, X.; Li, C. Photocatalytic Water Oxidation on $BiVO_4$ with the Electrocatalyst as an Oxidation Cocatalyst: Essential Relations between Electrocatalyst and Photocatalyst. *J. Phys. Chem. C* **2012**, *116*, 5082−5089.

(8) Liu, G.; Niu, P.; Sun, C. H.; Smith, S. C.; Chen, Z. G.; Lu, G. Q. (Max); Cheng, H. M. Unique Electronic Structure Induced High Photoreactivity of Sulfur-Doped Graphitic C_3N_4. *J. Am. Chem. Soc.* **2010**, *132*, 11642−11648.

(9) Liu, C.; Jing, L. Q.; He, L. M.; Luan, Y. B.; Li, C. M. Phosphate-modified Graphitic C_3N_4 as Efficient Photocatalyst for Degrading Colorless Pollutants by Promoting O_2 Adsorption. *Chem. Commun.* **2014**, *50*, 1999−2001.

(10) Kudo, A.; Miseki, Y. Heterogeneous Photocatalyst Materials for Water Splitting. *Chem. Soc. Rev.* **2009**, *38*, 253−278.

(11) Ding, C. M.; Shi, J. Y.; Wang, D. G.; Wang, Z. J.; Wang, N.; Liu, G. J.; Xiong, F. Q.; Li, C. Visible Light Driven Overall Water Splitting Using Cocatalyst/$BiVO_4$ Photoanode with Minimized Bias. *Phys. Chem. Chem. Phys.* **2013**, *15*, 4589−4595.

(12) Luan, Y. B.; Jing, L. Q.; Xie, Y.; Sun, X. J.; Feng, Y. J.; Fu, H. G. Exceptional Photocatalytic Activity of 001-Facet-Exposed TiO_2 Mainly Depending on Enhanced Adsorbed Oxygen by Residual Hydrogen Fluoride. *ACS Catal.* **2013**, *3*, 1378−1385.

(13) Pilli, S. K.; Deutsch, T. G.; Furtak, T. E.; Turner, J. A.; Brown, L. D.; Herring, A. M. Light Induced Water Oxidation on Cobalt-phosphate (Co−Pi) Catalyst Modified Semi-transparent, Porous SiO_2−$BiVO_4$ Electrodes. *Phys. Chem. Chem. Phys.* **2012**, *4*, 7032−7039.

(14) Chatchai, P.; Kishioka, S. Y.; Murakami, Y.; Nosaka, A. Y.; Nosaka, Y. Enhanced Photoelectrocatalytic Activity of FTO/WO_3/$BiVO_4$ Electrode Modified with Gold Nanoparticles for Water Oxidation under Visible Light Irradiation. *Electrochim. Acta* **2010**, *55*, 592−596.

(15) Ren, L.; Jin, L.; Wang, J. B.; Yang, F.; Qiu, M. Q.; Yu, Y. Template-free Synthesis of $BiVO_4$ Nanostructures: I. Nanotubes with Hexagonal Cross Sections by Oriented Attachment and Their Photocatalytic Property for Water Splitting under Visible Light. *Nanotechnology* **2009**, *20*, 115603 DOI: 10.1088/0957-4484/20/11/115603.

(16) Xi, G. C.; Ye, J. H. Synthesis of Bismuth Vanadate Nanoplates with Exposed (001) Facets and Enhanced Visible-light Photocatalytic Properties. *Chem. Commun.* **2010**, *46*, 1893−1895.

(17) Wang, Z. Q.; Luo, W. J.; Yan, S. C.; Feng, J. Y.; Zhao, Z. Y.; Zhu, Y. S.; Li, Z. S.; Zou, Z. G. $BiVO_4$ Nano−leaves: Mild Synthesis and Improved Photocatalytic Activity for O_2 Production under Visible Light Irradiation. *CrystEngComm.* **2011**, *13*, 2500−2504.

(18) Rao, P. M.; Cai, L. L.; Liu, C.; Cho, I. S.; Lee, C. H.; Weisse, J. M.; Yang, P. D.; Zheng, X. L. Simultaneously Efficient Light Absorption and Charge Separation in WO_3/$BiVO_4$ Core/Shell Nanowire Photoanode for Photoelectrochemical Water Oxidation. *Nano Lett.* **2014**, *14*, 1099−1105.

(19) Sun, Y. F.; Wu, C. Z.; Long, R.; Cui, Y.; Zhang, S. D.; Xie, Y. Synthetic Loosely Packed Monoclinic $BiVO_4$ Nanoellipsoids with Novel Multiresponses to Visible Light, Trace Gas and Temperature. *Chem. Commun.* **2009**, 4542−4544.

(20) Zhang, L. W.; Reisner, E.; Baumberg, J. J. Al-doped ZnO Inverse Opal Networks as Efficient electron Collectors in $BiVO_4$ Photoanodes for Solar Water Oxidation. *Energy Environ. Sci.* **2014**, *7*, 1402−1408.

(21) Ye, H.; Park, H. S.; Bard, A. J. Screening of Electrocatalysts for Photoelectrochemical Water Oxidation on W-Doped $BiVO_4$ Photocatalysts by Scanning Electrochemical Microscopy. *J. Phys. Chem. C* **2011**, *115*, 12464−12470.

(22) Yao, W. F.; Iwai, H.; Ye, J. H. Effects of Molybdenum Substitution on the Photocatalytic Behavior of $BiVO_4$. *Dalton Trans.* **2008**, 1426−1430.

(23) Jo, W. J.; Jang, J. W.; Kong, K.; Kang, H. J.; Kim, J. Y.; Jun, H.; Parmar, K. P. S.; Lee, J. S. Phosphate Doping into Monoclinic $BiVO_4$ for Enhanced Photoelectrochemical Water Oxidation Activity. *Angew. Chem.* **2012**, *124*, 3201−3205.

(24) Xie, M. Z.; Fu, X. D.; Jing, L. Q.; Luan, P.; Feng, Y. J.; Fu, H. G. Long-lived Visible-excited Charge Carriers of TiO_2/$BiVO_4$ Nanocomposite and Its Unexpected Photoactivity for Water Splitting. *Adv. Energy Mater.* **2013**, DOI: 10.1002/aenm.201300995.

(25) Ho-Kimura, S.; Moniz, S. J. A.; Handoko, A. D.; Tang, J. W. Enhanced Photoelectrochemical Water Splitting by Nanostructured $BiVO_4$-TiO_2 Composite Electrodes. *J. Mater. Chem. A* **2014**, *2*, 3948−3953.

(26) Tang, X. S.; Choo, E. S. G.; Li, L.; Ding, J.; Xue, J. M. Synthesis of ZnO Nanoparticles with Tunable Emission Colors and Their Cell Labeling Applications. *Chem. Mater.* **2010**, *22*, 3383−3388.
(27) Hong, Y.; Tian, C. G.; Jiang, B. J.; Wu, A. P.; Zhang, Q.; Tian, G. H.; Fu, H. G. Facile Synthesis of Sheet-like ZnO Assembly Composed of Small ZnO Particles for Highly Efficient Photocatalysis. *J. Mater. Chem. A* **2013**, *1*, 5700−5708.
(28) Tokunaga, S.; Kato, H.; Kudo, A. Selective Preparation of Monoclinic and Tetragonal $BiVO_4$ with Scheelite Structure and Their Photocatalytic Properties. *Chem. Mater.* **2001**, *13*, 4624−4628.
(29) Zhang, H.; Yang, D. R.; Ma, X. Y.; Du, N.; Wu, J. B.; Que, D. L. Straight and Thin ZnO Nanorods: Hectogram-Scale Synthesis at Low Temperature and Cathodoluminescence. *J. Phys. Chem. B* **2006**, *110*, 827−830.
(30) Hirano, M.; Ota, K.; Iwata, H. Direct Formation of Anatase (TiO_2)/Silica (SiO_2) Composite Nanoparticles with High Phase Stability of 1300 °C from Acidic Solution by Hydrolysis under Hydrothermal Condition. *Chem. Mater.* **2004**, *16*, 3725−3732.
(31) Xie, C.; Xu, Z. L.; Yang, Q. J.; Xue, B. Y.; Du, Y. G.; Zhang, J. H. Enhanced Photocatalytic Activity of Titania−silica Mixed Oxide Prepared via Basic Hydrolyzation. *J. Mater. Sci. Eng., B* **2004**, *112*, 34−41.
(32) Ge, J. P.; Zhang, Q.; Zhang, T. R.; Yin, Y. D. Core−Satellite Nanocomposite Catalysts Protected by a Porous Silica Shell: Controllable Reactivity, High Stability, and Magnetic Recyclability. *Angew. Chem.* **2008**, *120*, 9056−9060.
(33) Sun, W. T.; Xie, M. Z.; Jing, L. Q.; Luan, Y. B.; Fu, H. G. Synthesis of Large Surface Area Nano-sized $BiVO_4$ by an EDTA-modified Hydrothermal Process and Its Enhanced Visible Photocatalytic Activity. *J. Solid State Chem.* **2011**, *184*, 3050−3054.
(34) Becker, J.; Raghupathi, K. R.; Pierre, J. S.; Zhao, D.; Koodali, R. T. Tuning of the Crystallite and Particle Sizes of ZnO Nanocrystalline Materials in Solvothermal Synthesis and Their Photocatalytic Activity for Dye Degradation. *J. Phys. Chem. C* **2011**, *115*, 13844−13850.
(35) Liu, D. N.; Jing, L. Q.; Luan, P.; Tang, J. W.; Fu, H. G. Enhancement Effects of Cobalt Phosphate Modification on Activity for Photoelectrochemical Water Oxidation of TiO_2 and Mechanism Insights. *ACS Appl. Mater. Interfaces* **2013**, *5*, 4046−4052.
(36) He, L. M.; Jing, L. Q.; Li, Z. J.; Sun, W. T.; Liu, C. Enhanced Visible Photocatalytic Activity of Nanocrystallinea-Fe_2O_3 by Coupling Phosphate Functionalized Graphene. *RSC Adv.* **2013**, *3*, 7438−7444.
(37) Radovanovic, P. V.; Norberg, N. S.; McNally, K. E.; Gamelin, D. R. Colloidal Transition-Metal-Doped ZnO Quantum Dots. *J. Am. Chem. Soc.* **2002**, *124*, 15192−15193.
(38) Jing, L. Q.; Cao, Y.; Cui, H. Q.; Durrant, J. R.; Tang, J. W.; Liu, D. N.; Fu, H. G. Acceleration Effects of Phosphate Modification on the Decay Dynamics of Photo-generated Electrons of TiO_2 and Its Photocatalytic Activity. *Chem. Commun.* **2012**, *48*, 10775−10777.
(39) Hayoun, R.; Whitaker, K. M.; Gamelin, D. R.; Mayer, J. M. Electron Transfer Between Colloidal ZnO Nanocrystals. *J. Am. Chem. Soc.* **2011**, *133*, 4228−4231.
(40) Kang, C. H.; Jing, L. Q.; Guo, T.; Cui, H. C.; Zhou, J.; Fu, H. G. Mesoporous SiO_2-Modified Nanocrystalline TiO_2 with High Anatase Thermal Stability and Large Surface Area as Efficient Photocatalyst. *J. Phys. Chem. C* **2009**, *113*, 1006−1013.
(41) Xie, B. P.; Zhang, H. X.; Cai, P. X.; Qiu, R. L.; Xiong, Y. Simultaneous Photocatalytic Reduction of Cr(VI) and Oxidation of Phenol over Monoclinic $BiVO_4$ under Visible Light Irradiation. *Chemosphere* **2006**, *63*, 956−963.
(42) Barpuzary, D.; Khan, Z.; Vinothkumar, N.; De, M.; Qureshi, M. Hierarchically Grown Urchinlike CdS@ZnO and CdS@Al_2O_3 Heteroarrays for Efficient Visible-Light-Driven Photocatalytic Hydrogen Generation. *J. Phys. Chem. C* **2012**, *116*, 150−156.